EUROPEAN JOURNAL OF COMPUTATIONAL MECHANICS, 2017
VOL. 26, NOS. 5–6, 525–540
https://doi.org/10.1080/17797179.2017.1379863

Taylor & Francis
Taylor & Francis Group



# Fast BEM multi-domain approach for the elastostatic analysis of short fibre composites

R. Q. Rodriguez[a‡], A. F. Galvis[a], P. Sollero[a], C. L. Tan[b] and E. L. Albuquerque[c]

[a]Department of Computational Mechanics, School of Mechanical Engineering, University of Campinas, Campinas, Brazil; [b]Department of Mechanical and Aerospace Engineering, Carleton University, Ottawa, Canada; [c]Faculty of Technology, Department of Mechanical Engineering, University of Brasilia, Brasilia, Brazil

**ABSTRACT**

Composite materials are usually treated as homogeneous when carrying out structural design. However, failure in these materials often originated at their heterogeneous microstructure or constituents; hence, the different materials should be considered in the analysis. The use of composite materials has increased considerably over the years due to their relative superior properties. The accurate determination of their mechanical properties and behaviour is thus of great practical significance. The Boundary Element Method (BEM) has demonstrated to be a powerful computational technique for the analysis of many physical and engineering problems. The present work deals with the use of the multi-domain BEM to obtain a more appropriate characterisation of fibre–matrix composites. The generally anisotropic fundamental solution based on a double-Fourier series is employed together with a fast BEM approach, namely, the Adaptive Cross Approximation (ACA) technique. The ACA technique is aimed at speeding up the process required to generate the BEM matrices. Some numerical examples are presented to demonstrate its applicability. The present work is a precursor to treating problems involving anisotropic inclusions in general composites.

**ARTICLE HISTORY**
Received 1 August 2017
Accepted 12 September 2017

**KEYWORDS**
Boundary element method; composites; anisotropy; Fourier series; adaptive cross approximation

## 1. Introduction

The use of composite materials in engineering has increased due to their relative superior properties such as lightness, flexibility, durability, adaptability and mechanical resistance. Hence, accurately predicting the behaviour and determining its mechanical properties is of great importance. Fibre–matrix composites are one of the most common types of composites due to its particular composition and properties. For example, the addition of high strength fibres to a polymer

**CONTACT** P. Sollero sollero@fem.unicamp.br
‡Present address: School of Civil Engineering, State University of Mato Grosso campus Tangará da Serra, Tangará da Serra 78300-000, MT, Brazil.

matrix can greatly improve some of its mechanical properties such as the ultimate tensile strength, impact resistance, temperature resistance, among others.

The BEM is a well-established and powerful computational technique for the analysis of many physical and engineering problems. Its implementation for elastostatics involves the evaluation of the displacement fundamental solution and its derivatives. For the case of isotropic materials, it can be represented by simple explicit forms. However, the corresponding expressions for the case of generally anisotropic solids are significantly more complex and mathematically involved.

The anisotropic fundamental solution for displacements was first presented by Lifshitz and Rozenzweig (1947), but not as a closed form. It was expressed as a contour integral around a unit circle on a oblique plane at the field point and in terms of the Christoffel tensor. The first implementation of this solution into a 3D BEM code was by Wilson and Cruse (1978). There were significant challenges in the development of efficient algorithms for the accurate numerical evaluation of this quantity and its derivatives (see Phan, Gray, & Kaplan, 2004; Sales & Gray, 1998; Tonon, Pan, & Amadei, 2001; Wang & Denda, 2007). Explicit, closed form expressions of the Green's function and its derivatives were derived by Ting and Lee (1997), and Lee (2003) in terms of the Stroh's eigenvalues. However, they were left unnoticed by the BEM community until Tavara, Ortiz, Mantic, and Paris (2008) implemented it in BEM for the special case of transverse isotropy, and Shiah, Tan, and Lee (2008) and Tan, Shiah, and Lin (2009) for general anisotropy. Taking advantage of the periodic nature of the Green's function, when expressed in spherical coordinates, Shiah, Tan, and Wang (2012), reformulated this fundamental solution and its derivatives by representing them by double-Fourier series. Recently, Tan, Shiah, and Wang (2013) further implemented it into a 3D BEM code. This development reduced significantly the computational effort for the evaluation of these quantities.

The final matrix system in BEM analysis is generally fully populated and unsymmetric. For very large numerical problems, such as when solving multi-scale problems, the memory requirements and solution times may be less than desirable. The issue of speeding up the solution process of large system of equations has been addressed by Rokhlin (1985), Bebendorf (2000), Bebendorf and Rjasanow (2003). As stated in Bebendorf and Rjasanow (2003), it is possible to use purely algebraic algorithms to generate the approximation of suitable blocks of the collocation matrix, using only relatively few entries of the original blocks. This technique is referred to as the Adaptive Cross Approximation (ACA). The ACA uses matrix hierarchisation to reduce the storage requirement and the computational complexity arising in the numerical analysis.

In this work, the application of hierarchical matrices and ACA to short fibre–matrix problems using the 3D multi-domain BEM for elastostatics with the anisotropic fundamental solution based on double-Fourier series is illustrated. First, this anisotropic fundamental solution and its derivatives are reviewed.

Then, the use of hierarchical matrices and ACA is discussed. This will be followed by some numerical examples that will show the applicability of the proposed methodology.

## 2. 3D anisotropic fundamental solutions and its derivatives

The displacement fundamental solution or Green's function, $\mathbf{U}(\mathbf{x}) = U_{ij}(P, Q)$, is defined as the displacement response in the $x_i$ direction at the field point $Q$ due to a unit load applied in the $x_j$ direction at the source point $P$ in an homogeneous infinite body. This solution for the case of 3D generally anisotropic materials was firstly derived by Lifshitz and Rozenzweig (1947). Ting and Lee (1997) showed that the Green's function can be also expressed in terms of the Barnett–Lothe tensor, $\mathbf{H}[\mathbf{x}]$. In the solution first derived by Lifshitz and Rozenzweig (1947), $\mathbf{H}[\mathbf{x}]$ is expressed considering a spherical coordinate system, the explicit form of the Green's function can be expressed as follows,

$$\mathbf{U}\left(r,\theta,\phi\right) = \frac{1}{4\pi r}\mathbf{H}\left(\theta,\phi\right). \tag{1}$$

This expression depends only on the spherical angles $(\theta, \phi)$ and can be further expressed in terms of the Stroh's eigenvalues as,

$$\mathbf{H}\left(\theta,\phi\right) = \frac{1}{|\mathbf{T}|}\sum_{n=0}^{4} q_n \hat{\Gamma}^{(n)}, \tag{2}$$

where $\hat{\Gamma}$ is the adjoint of $\Gamma$. The Stroh's eigenvalues are obtained solving a sextic equation in $p$, which is obtained from setting the determinant $|\Gamma(p)|$ to zero. The explicit expressions for $|\mathbf{T}|$, $\Gamma$ and $q_n$ can be found in Ting and Lee (1997) and Tan et al. (2013). Moreover, due to its periodic nature, $\mathbf{H}\left(\theta,\phi\right)$ can be represented by double-Fourier series around $\theta$ and $\phi$, as follows,

$$\begin{aligned} H_{uv}\left(\theta,\phi\right) &= \sum_{m=-\infty}^{\infty}\sum_{n=-\infty}^{\infty} \lambda_{uv}^{(m,n)} e^{i\left(m\theta+n\phi\right)}, \quad (u,v=1,2,3), \\ \lambda_{uv}^{(m,n)} &= \frac{1}{4\pi^2}\int_{-\pi}^{\pi}\int_{-\pi}^{\pi} H_{uv}\left(\theta,\phi\right) e^{-i\left(m\theta+n\phi\right)}\mathrm{d}\theta\,\mathrm{d}\phi, \end{aligned} \tag{3}$$

where $\lambda_{uv}^{(m,n)}$ are the Fourier coefficients, which can be numerically integrated by, e.g. Gaussian quadrature. The $k$ abscissa points, $\lambda_{uv}^{(m,n)}$, may be re-written as,

$$\lambda_{uv}^{(m,n)} = \frac{1}{4}\sum_{p=1}^{k}\sum_{q=1}^{k} w_p w_q f_{uv}^{(m,n)}\left(\pi\xi_p, \pi\xi_q\right), \tag{4}$$

where $w$ and $\xi$ are the weights and Gauss points, respectively, and $f_{uv}^{(m,n)}\left(\theta,\phi\right)$ represents the integrand of $\lambda_{uv}^{(m,n)}$. In short, the fundamental displacement solu-

tion can also be written as,

$$U_{uv}\left(r,\theta,\phi\right)=\frac{1}{4\pi r}\sum_{m=-\alpha}^{\alpha}\sum_{n=-\alpha}^{\alpha}\lambda_{uv}^{(m,n)}e^{i\left(m\theta+n\phi\right)}, \tag{5}$$

where $\alpha$ is an integer number, large enough to yield the desired accuracy. Numerical experiments reported in Tan et al. (2013) have shown that values of $k = 64$ and $\alpha = 16$ will be adequate to evaluate even the most highly anisotropic materials. Lee (2009), using partial differentiations of the Green's function in spherical coordinates, eliminated the necessity of working with high order tensors, as those seen in Ting and Lee (1997) and Lee (2003). The displacement derivatives can be obtained by working in spherical coordinates and applying the chain rule. All explicit forms are given in Shiah et al. (2012), Tan et al. (2013), Shiah, Tan, and Lee (2010). The most significant advantage of using this Fourier series representation of the Green's function and its derivatives is that the Fourier series coefficients, $\lambda_{uv}^{(m,n)}$, are only evaluated once. This further reduces the computational effort, besides the relatively simplicity of the implementation into a BEM code.

## 3. Acceleration scheme for the BEM

The proposed acceleration scheme has as its main objective the reduction of the memory requirements as well as to speed up the total solution time. The scheme takes advantage of the matrix hierarchisation and the use of low rank approximations by the use of the ACA technique. The matrix is represented as a collection of blocks, some of which admit a particular approximated representation that can be obtained by computing only few entries from the original blocks. These special blocks are called admissible or low rank blocks and are obtained by the ACA. Blocks that cannot be represented in this way must be computed and stored entirely, as stated by Benedetti, Milazzo, and Aliabadi (2009, 2011).

In BEM analysis, the kernels of the BIE are computed and they are the coefficients of the system matrices. In a potential theory problem, the kernels are the potential and flux fundamental solutions, while in an elasticity problem, the kernels are the displacement $U_{jk}$ and traction $T_{jk}$ fundamental solutions. They both depend upon the positions of the source point $\mathbf{d}$ and the field point $\mathbf{x}$. The kernels $U_{jk}(\mathbf{d},\mathbf{x})$ and $T_{jk}(\mathbf{d},\mathbf{x})$ are two-point asymptotic smooth functions and singular when $\mathbf{d} = \mathbf{x}$. These functions can be approximated by a sum of products of two functions $u_i(\mathbf{d})$ and $v_i(\mathbf{x})$,

$$\kappa\left(\mathbf{d},\mathbf{x}\right)=\sum_{i=1}^{k}u_i\left(\mathbf{d}\right)v_i\left(\mathbf{x}\right)+R_\kappa\left(\mathbf{d},\mathbf{x}\right), \tag{6}$$

where $\kappa$ can be either $u_{jk}$ or $t_{jk}$, $R_\kappa(\mathbf{d},\mathbf{x})$ is the error of the approximation and $\left|R_\kappa\left(\mathbf{d},\mathbf{x}\right)\right|\leq\varepsilon_\kappa$ with $\varepsilon_\kappa\to 0$ for $k\to 0$.

The existence of low rank approximants is based on the asymptotic smoothness of the kernel functions, i.e. on the fact that kernels $U_{ij}$ and $T_{ij}$ are singular only when the source and field points are coincident, when $\mathbf{x} = \mathbf{y}$, Bebendorf (2000), Bebendorf and Rjasanow (2003), and Grasedyck (2005). This is a sufficient condition for the existence of low rank approximants. A low rank block $M$ of size $m$ x $n$ has the following representation

$$M_k = \sum_{i=1}^{k} a_i \cdot b_i{}^{\mathrm{T}} = A \cdot B^{\mathrm{T}}, \tag{7}$$

where $A$ and $B$ are matrices of size $m$ x $k$ and $n$ x $k$, respectively. If $k$ is low, the representation shown above requires the storage of $(m + n)k$ real numbers instead of $m$ x $n$, speeding up the matrix–vector product of the corresponding block. For a more detailed analysis, refer to Borm, Grasedick, and Hackbusch (2003) and Grasedyck and Hackbusch (2003).

The approximation block $M_k$ satisfies the relation $\|M - M_k\|_F \leq \varepsilon \|M\|_F$, where $\|\cdot\|_F$ represents the Frobenius norm and $\varepsilon$ is the prescribed relative error. The low rank blocks are constructed by computing and storing only some of the original blocks entries. Such entries allow the representation presented in equation (7) through suitable algorithms, namely, the ACA.

Large dense matrices with diagonal singularity can be hierarchical approximated following the three basic steps (Kurz, Rain, & Rjasanow, 2007):

(1) construction of clusters,
(2) finding possible admissible blocks and,
(3) low rank approximation of admissible blocks.

Kurz et al. (2007) adapted the ACA algorithm proposed by Bebendorf (2000) and applied it with BEM. An implementation of this algorithm in conjunction with the double-Fourier fundamental solutions is presented in this work. First, the mass and centre of each cluster are stored, then, the covariance matrix of the cluster is obtained by

$$C = \sum_{k=1}^{n} g_k \left(x_k - X\right) \left(x_k - X\right)^{\mathrm{T}}, \tag{8}$$

where $n$ is the number of elements of the cluster, $g_k$ is the element area (length for 2D problems) and $X$ is the centre of the cluster.

Then, the largest eigenvalue of $C$ defines the eigenvector, $v_1$, which gives the direction of the longest extension of the cluster. The separation plane (line in 2D) $\left\{\mathbf{x} \in \Re^3 : (\mathbf{x} - X, v_1) = 0\right\}$ goes through the centre $X$ of the cluster and is orthogonal to $v_1$. The algorithm is applied recursively to the sons until they contain less than or equal to some prescribed number $n_{\min}$ of elements. Next, cluster pairs which are geometrically well separated are identified. They will be

regarded as admissible cluster pairs. An appropriate admissibility criterion is the following simple geometrical condition. A pair of clusters $(Cl_x, Cl_y)$ with $n_x > n_{\min}$ and $m_y > n_{\min}$ elements is admissible if,

$$\min(\text{diam}(Cl_x), \text{diam}(Cl_y)) \leq \eta \text{dist}(Cl_x, Cl_y), \tag{9}$$

where $\text{diam}(Cl_x)$ is the diameter of the circumscribed sphere evolving the cluster $Cl_x$, $\text{dist}(Cl_x, Cl_y)$ is the distance between clusters and $\eta$ is called the admissibility parameter. This parameter influences the number of admissible blocks on one hand and the convergence speed of the adaptive approximation of low rank blocks on the other hand (Borm et al., 2003). A full study of this parameter was assessed by Benedetti et al. (2011) and Rodríguez, Galvis, Sollero, and Albuquerque (2013). They showed that the choice of $\eta$ directly affects the quality of the ACA-generated matrix and a good choice of this parameter results in a matrix closer to the optimal matrix produced by the coarsening procedure. This fact was also justified by the reduction in the number of blocks. Once the clusters were defined and all admissible blocks were detected, the ACA was used to approximate these blocks by low rank.

## 4. Multi-domain applied to 3D fibre–matrix problems

The multi-domain BEM approach is a natural choice when solving fibre–matrix problems, due to the possibility of analysing each region individually. After the BEM is applied to each sub-region, or sub-domain, the system coupling can be formulated by considering displacement compatibility and traction equilibrium at the interfaces between sub-regions. The compatibility condition requires that nodal displacements for a region $i$, at an interface between region $i$ and region $j$, must be equal to the displacement components evaluated in region $j$ at the same interface. The equilibrium between traction vectors at the interface nodes must be also considered. These conditions can be represented as,

$$\begin{aligned} \mathbf{u}^i &= \mathbf{u}^j \\ \mathbf{t}^i &= \mathbf{t}^j \end{aligned} \tag{10}$$

where the double subscripts is used to denote the vector in question is a collection of components on the interface between region $i$ and region $j$. Further details on the multi-domain approach can be found in Kane (1994) and Aliabadi (2002). As an illustration of the current implementation, consider the simple example with four fibres shown in Figure 1.

Five regions were created from the above example; the matrix and the four fibres. The multi-domain collocation matrix, $\mathbf{H}_{coll}$, generated in this example is shown below.

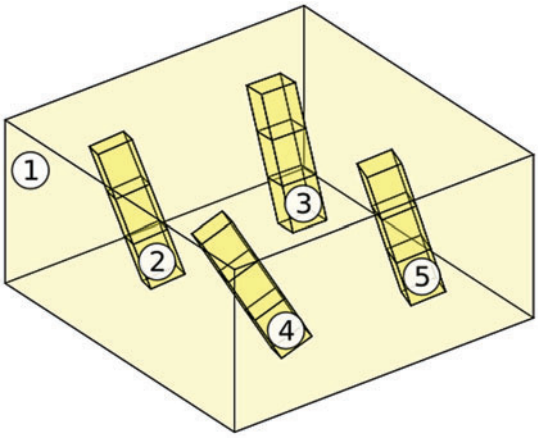


**Figure 1.** Multi-domain example with four fibres.

$$\begin{bmatrix} \mathbf{H}_{11}^{1} & \mathbf{H}_{12}^{1} & \mathbf{H}_{13}^{1} & \mathbf{H}_{14}^{1} & \mathbf{H}_{15}^{1} & -\mathbf{G}_{12}^{1} & -\mathbf{G}_{13}^{1} & -\mathbf{G}_{14}^{1} & -\mathbf{G}_{15}^{1} \\ \mathbf{0} & \mathbf{H}_{12}^{2} & \mathbf{0} & \mathbf{0} & \mathbf{0} & \mathbf{G}_{12}^{2} & \mathbf{0} & \mathbf{0} & \mathbf{0} \\ \mathbf{0} & \mathbf{0} & \mathbf{H}_{13}^{3} & \mathbf{0} & \mathbf{0} & \mathbf{0} & \mathbf{G}_{13}^{3} & \mathbf{0} & \mathbf{0} \\ \mathbf{0} & \mathbf{0} & \mathbf{0} & \mathbf{H}_{14}^{4} & \mathbf{0} & \mathbf{0} & \mathbf{0} & \mathbf{G}_{14}^{4} & \mathbf{0} \\ \mathbf{0} & \mathbf{0} & \mathbf{0} & \mathbf{0} & \mathbf{H}_{15}^{5} & \mathbf{0} & \mathbf{0} & \mathbf{0} & \mathbf{G}_{15}^{5} \end{bmatrix} \tag{11}$$

where $\mathbf{H}_{ij}^{e}$ and $\mathbf{G}_{ij}^{e}$ represent the incidences in matrices $\mathbf{H}$ and $\mathbf{G}$ between sub-regions $i$ and $j$ in the case where quantities are associated to a specific region $e$. The order of the sub-region incidences are determined by first simply listing all the permutations, (Kane, 1994), for this example,

$$11\ 12\ 13\ 14\ 15\ 21^{*}\ 22\ 23\ 24\ 25 \cdots 51^{*}\ 52^{*}\ 53^{*}\ 54^{*}\ 55 \tag{12}$$

where the digits represent the subregions being analysed. For the permutation where the first digit is higher than the second digit (*), blocks of traction components, $\mathbf{G}_{ij}^{e}$, are created; otherwise, blocks of displacement components, $\mathbf{H}_{ij}^{e}$, are created. The negative sign is due to the traction having opposite signs when analysing different regions at the interface. Moreover, as there is no contact between fibres, matrices with both indices $i$ and $j$ corresponding to fibres are equal to zero. In this case all fibres are within them matrix, therefore subregions $i = j$ for $i > 1$ do not occur. Hence, the system can be further compressed as,

$$\mathbf{H}_{coll} = \left[\mathbf{A}\ \mathbf{C}\right], \tag{13}$$

where,

$$\mathbf{A} = \begin{bmatrix} \mathbf{H}_{11}^{1} & \mathbf{H}_{12}^{1} & \mathbf{H}_{13}^{1} & \mathbf{H}_{14}^{1} & \mathbf{H}_{15}^{1} \\ \mathbf{0} & \mathbf{H}_{12}^{2} & \mathbf{0} & \mathbf{0} & \mathbf{0} \\ \mathbf{0} & \mathbf{0} & \mathbf{H}_{13}^{3} & \mathbf{0} & \mathbf{0} \\ \mathbf{0} & \mathbf{0} & \mathbf{0} & \mathbf{H}_{14}^{4} & \mathbf{0} \\ \mathbf{0} & \mathbf{0} & \mathbf{0} & \mathbf{0} & \mathbf{H}_{15}^{5} \end{bmatrix}, \tag{14}$$

and

$$\mathbf{C} = \begin{bmatrix} -\mathbf{G}_{12}^{1} & -\mathbf{G}_{13}^{1} & -\mathbf{G}_{14}^{1} & -\mathbf{G}_{15}^{1} \\ \mathbf{G}_{12}^{2} & \mathbf{0} & \mathbf{0} & \mathbf{0} \\ \mathbf{0} & \mathbf{G}_{13}^{3} & \mathbf{0} & \mathbf{0} \\ \mathbf{0} & \mathbf{0} & \mathbf{G}_{14}^{4} & \mathbf{0} \\ \mathbf{0} & \mathbf{0} & \mathbf{0} & \mathbf{G}_{15}^{5} \end{bmatrix} \tag{15}$$

The sub-matrices, $\mathbf{H}_{ij}^{e}$ and $\mathbf{G}_{ij}^{e}$, are obtained applying the BEM to each $e$ region individually. The ACA technique can also be used to this end. It is worth to point out that, usually, the fibres have a very small number of elements and consequently the ACA would not present any advantage on the approximation. Thus, the ACA will be applied to the region which contains the matrix medium. For regular multi-domain problems no compression can be made and the system of equation (11) should be used instead.

## 5. Numerical examples

Three numerical examples are presented to demonstrate the successful implementation of the proposed BEM approach with the ACA acceleration scheme described above. In the first example, a square cross-section beam under transverse pressure is analysed. Four regions are defined with the same material in order to test the multi-domain approach. Normalised displacements are compared with the continuous one-region BEM. In the second example, the fibre–matrix model is tested with an isotropic material. Results are compared with the analytical solution. Finally, the fibre–matrix model is tested with a more complex geometric combination of materials. The main objective is to test the acceleration scheme. Displacements are compared between conventional BEM and results obtained after applying the fast BEM approach. Moreover, the application of the ACA is tested by comparing the solution CPU times. It should be noted that materials for the problems treated are isotropic and transversely isotropic even though they are analysed using the BEM program for general anisotropy. The present work serves as a precursor to treating problems involving anisotropy inclusion in a matrix medium.

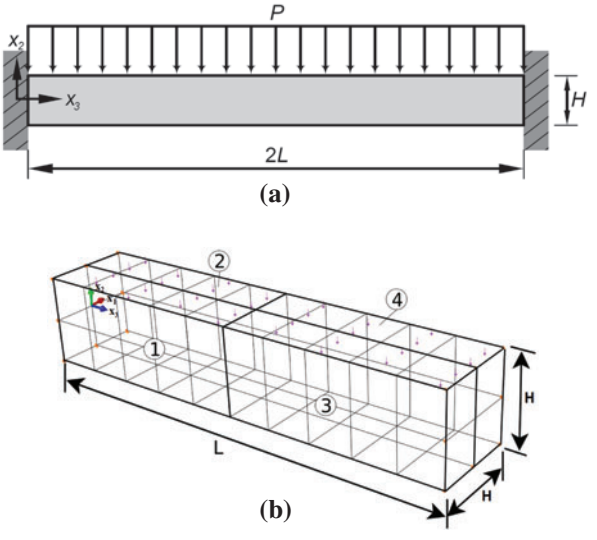


**Figure 2.** (a) Geometry and boundary conditions for example A; (b) multidomain BEM mesh of half beam.

### 5.1. Example a: multidomain with four regions

In this example, the multidomain approach for more than two regions is tested with quadratic discontinuous element. A short beam of length $2L$, square cross-section of side $H$ and $L = 5H$, is subjected to a uniformly distributed pressure load on its top surface, as shown in Figure 2(a). Figure 2(b) shows the BEM mesh for half of the beam that was modelled, taking advantage of symmetry. It consists of four sub-regions.

Each region has 34 quadratic discontinuous elements; a total of 136 elements, 305 geometrical nodes and 1088 physical nodes were used to model this problem. The anisotropic 3D formulation based on Fourier series was used for an isotropic material with $E = 1$ and $\nu = 0$. For the double-Fourier fundamental solution, $\alpha = 16$ and 64 Gauss integration points were used. Normalised transverse displacements along the $x_2$ direction for the four regions are shown in Figure 3.

Finally, displacements at nodes $(0.5, 0.5, x_3)$ are compared with results obtained from the conventional BEM with quadratic continuous elements and the analytical solution, as shown in Figure 4.

Good agreement was observed when both approaches were compared. Discontinuous quadratic elements were applied due to its simpler implementation when dealing with more than two regions in the multidomain approach and when debonding between elements occur.

### 5.2. Example B: short fibre–matrix model (Isotropy check)

In this example, the fibre–matrix model was implemented and tested. A general mesh generator was implemented. The fibres can be randomly oriented, as

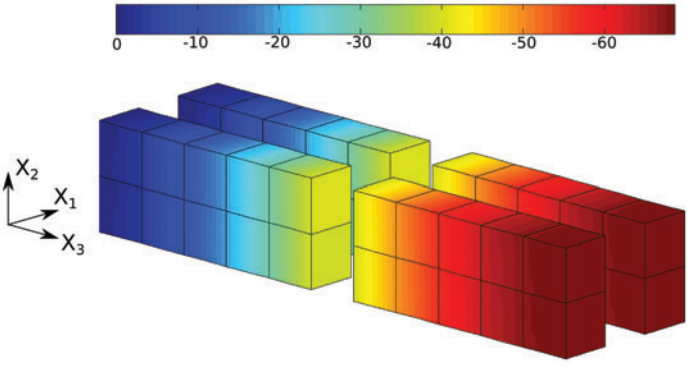


**Figure 3.** Normalised transverse $x_2$ displacement for the four regions.

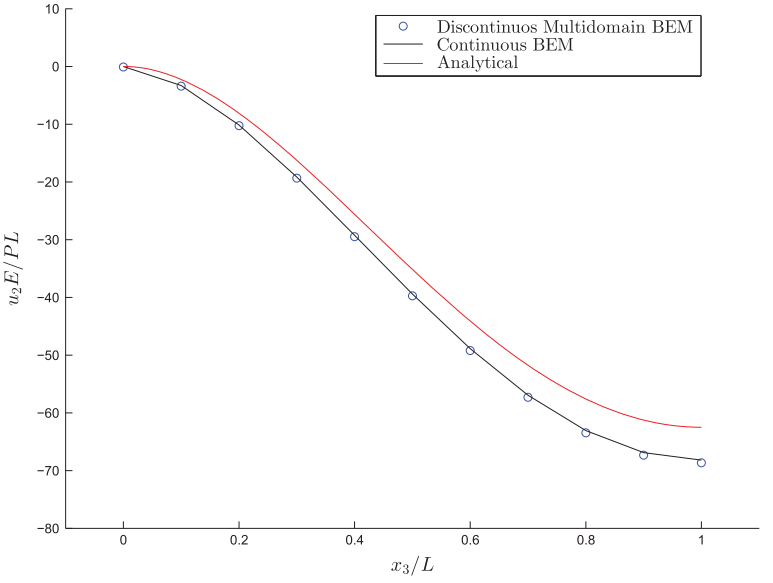


**Figure 4.** Normalised transverse displacement comparison at $(0.5, 0.5, x_3)$.

shown in Figure 5. The length and cross-section of the short fibres are also input parameters; thus, the fraction volume can be also imposed. A fibre–matrix model with 36 short fibres is shown in Figure 5(a), while a unit cell is shown in Figure 5(b).

First, the model was tested with an isotropic material with $E = 10{,}000$ and $\nu = 0.3$ for the short fibres and the matrix medium, however, the anisotropic 3D fundamental solution based on Fourier series was used. As usual, $\alpha = 16$ and 64 Gauss integration points were used for the Fourier representation. An isotropic material was used in order to properly compare results with the analytical solution. For this first fibre–matrix example, a bar of length 4 units and square cross-section of one unit in length is subjected to a uniformly distributed pressure load, $P = 1$, on its top surface, while, its bottom surface is restricted in the three

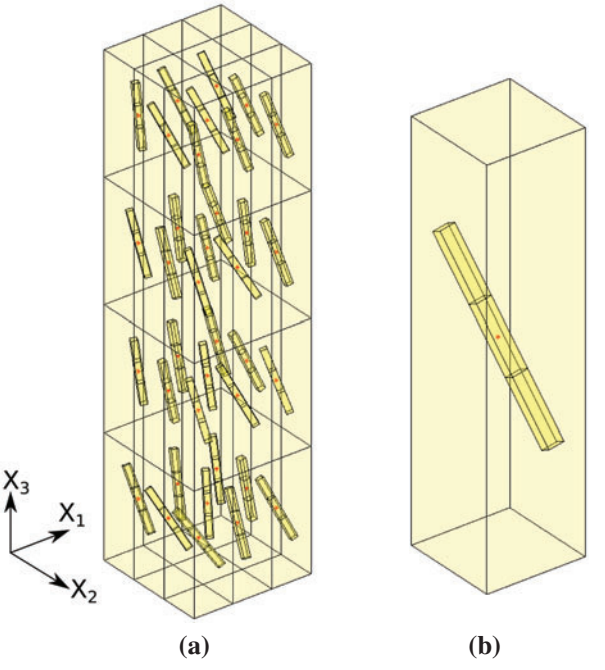


**Figure 5.** (a) Fibre–Matrix model with 36 fibres; (b) unit cell with a randomly oriented short fibre.

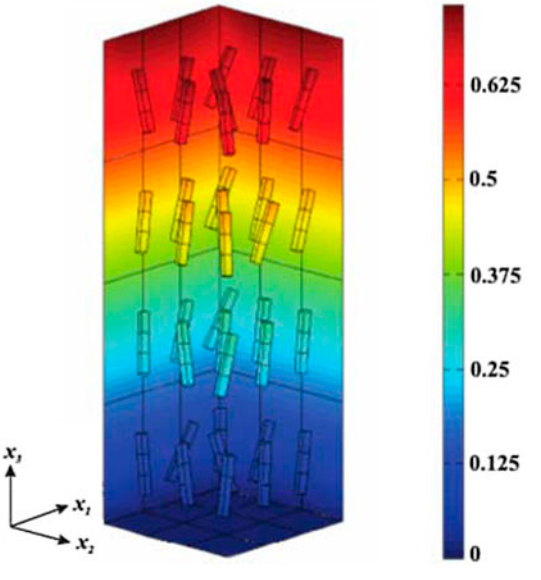


**Figure 6.** Normalised $x_3$ displacement in an isotropic fibre–matrix model.

coordinate directions. The simple analytical solution for the $u_3$ displacement is $Px_3/E$. Displacements along the $x_3$ direction for the fibre–matrix model are shown in Figure 6.

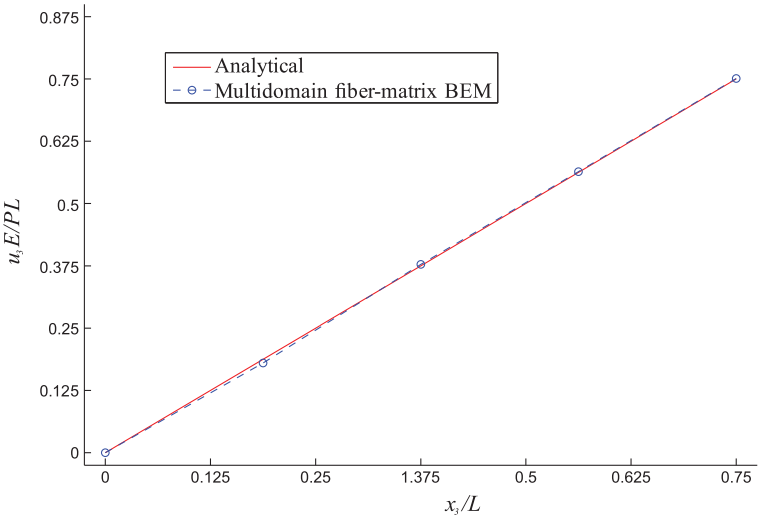


**Figure 7.** Numerical comparison of the normalised $x_3$ displacement with the analytical solution.

Displacements at nodes $(0.5, 0.5, x_3)$u are compared with the analytical solution, as shown in Figure 7.

Good agreement was observed when the fibre–matrix multidomain model was compared with the analytical solution.

### 5.3. Example C: ACA applied to more realistic model

In this example, the short fibre–matrix model is shown with a more realistic combination of materials for both, fibre and matrix. Furthermore, the ACA method was applied in the generation of BEM matrices **H** and **G**. For the matrix medium, a 3501-6 epoxy was considered. Material properties were considered as isotropic with $E = 4.2$ GPa and Poisson ratio $\nu = 0.34$. For the short fibres, a AS4 carbon material was considered. Material properties were considered as transversely isotropic with $E_1 = 225$ GPa, $E_2 = 15$ GPa, $G_{12} = 15$ GPa and $\nu_{12} = 0.2$. More details on the properties of the chosen combination fibre–matrix can be found in Soden, Hinton, and Kaddour (1998).

In this example, a bar of length 3 units and square cross-section with side length of unity was subjected to a uniformly distributed pressure load, $P = 1$, on its top surface, while, its bottom surface is restricted in the 3 coordinate directions. In order to test the ACA method, five different cases were analysed (4, 8, 12, 18 and 27 fibres). The ACA error tolerance is set to $\epsilon_c = 10^{-4}$. The maximum number of elements per cluster was set to 30 and the admissibility parameter, $\eta$, to 0.9. More details of the choice of these parameters are available in Benedetti et al. (2009) and Rodríguez et al. (2013). For the most refined case (27 fibres, 6480 quadratic discontinuous nodes) there were 45 clusters and 487 blocks, from which 46 were admissible pairs. Results from the BEM anisotropic multidomain model using the ACA for the $u_3$ displacement are shown in Figure 8.

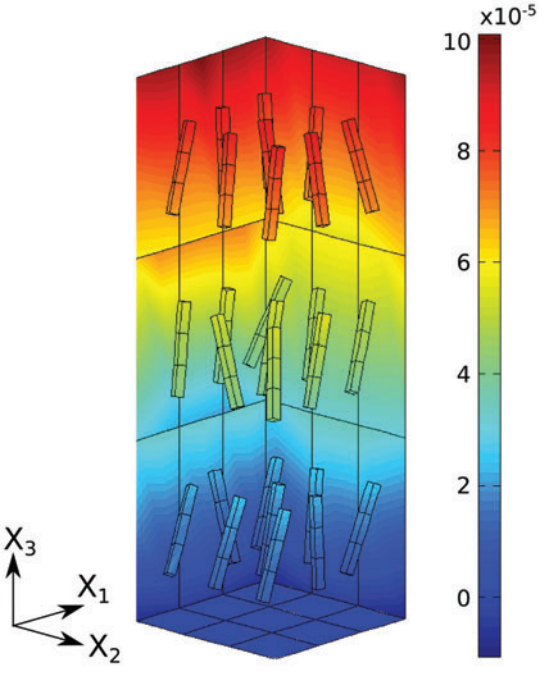


**Figure 8.** Displacement in the $x_3$ direction for the most refined mesh.

**Table 1.** Coordinates of the random nodes.

| Node | Coordinates $(x, y, z)$ |
|---|---|
| 349 | (0.000, 0.176, 1.050) |
| 841 | (0.163, 0.528, 0.577) |
| 1050 | (0.209, 0.509, 2.412) |
| 3439 | (0.791, 0.817, 2.583) |
| 6052 | (0.715, 0.585, 2.696) |

**Table 2.** Nodal comparison between conventional BEM and ACA for random nodes.

| | BEM | ACA | BEM | ACA | BEM | ACA |
|---|---|---|---|---|---|---|
| Node | $u_1 \times 10^{-6}$ | $u_1 \times 10^{-6}$ (Err.%) | $u_2 \times 10^{-6}$ | $u_2 \times 10^{-6}$ (Err.%) | $u_3 \times 10^{-4}$ | $u_3 \times 10^{-4}$ (Err.%) |
| 349 | −0.4341 | −0.4325 (0.37) | 26.750 | 26.790 (0.15) | 0.2916 | 0.2912 (0.14) |
| 841 | 1.5440 | 1.5470 (0.19) | −0.8381 | −0.8246 (1.61) | 0.1564 | 0.1564 (0.00) |
| 1050 | 1.1260 | 1.1270 (0.09) | −0.2478 | −0.2321 (6.34) | 0.7561 | 0.7562 (0.01) |
| 3439 | −0.2270 | −0.2335 (2.86) | −5.1020 | −5.0660 (0.71) | 0.7826 | 0.7829 (0.04) |
| 6052 | −0.5833 | −0.5849 (0.27) | −0.5269 | −0.5118 (2.87) | 0.8506 | 0.8508 (0.02) |

Table 2 shows comparison of the computed displacements $u_1$, $u_2$ and $u_3$ between conventional BEM and ACA. Five random nodes (349, 841, 1050, 3439 and 6052) were chosen for the comparison, as can be seen in Table 1.

The percentage discrepancies of the numerical results are also as indicated in the Table 2.

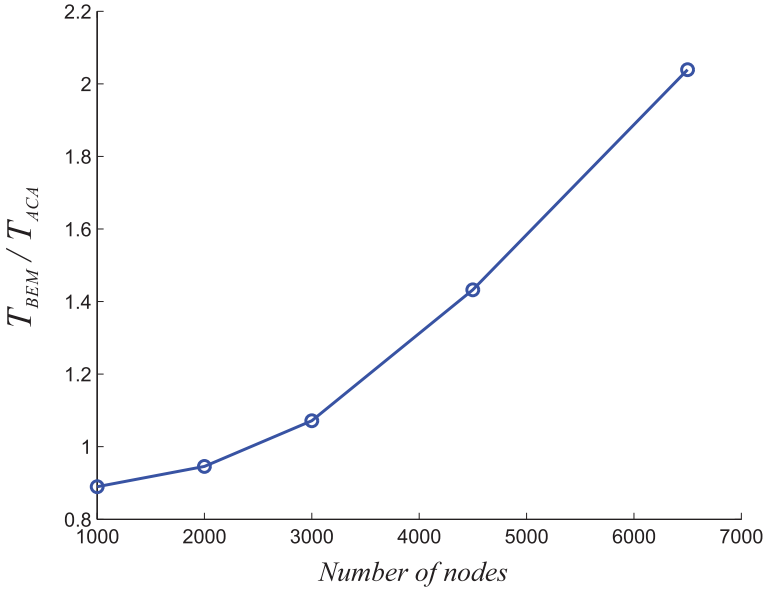


**Figure 9.** Variation of the speed up ratio $T_{\text{BEM}}/T_{\text{ACA}}$ between conventional BEM and ACA.

The maximum discrepancy was 6.34% for the displacement in the $x_2$-direction at node 1050. For this case, the displacement was $-0.2478 \times 10^{-6}$ mm for the conventional BEM, being substantially less than the ACA tolerance of $\epsilon_c = 10^{-4}$. As pointed out by Benedetti, Milazzo, and Aliabadi (2011), the ACA tolerance should be set to be compatible with the expected smallest response value.

Figure 9 shows the variation of the speed up ratio $T_{\text{BEM}}/T_{\text{ACA}}$ between CPU time for generating BEM matrices for conventional BEM $T_{\text{BEM}}$ and when the ACA method is applied $T_{\text{ACA}}$. It can be noted that when the numerical problem size gets to be large, the ACA scheme becomes more efficient than the conventional BEM.

## 6. Conclusions

In this work, the use of hierarchical matrices and low-rank approximations applied to 3D short fibre–matrix problems which employs the double-Fourier series representation of the Green's functions in multi-domain BEM analysis has been presented. Low rank approximations were accomplished by the use of ACA. This method is suitable for memory and time savings, especially in the case of large-scale problems. Moreover, the multi-domain approach was modified to account for short fibre–matrix problems. Results for a more realistic combination of fibre–matrix were also shown; they demonstrated that the ACA works better beyond a certain number of elements in the mesh. Beyond this level of discretisation, the CPU solution time using the ACA scheme will be less than

the conventional BEM formulation. The present study serves as a precursor to treating more general anisotropic inclusions in a matrix medium.

## Disclosure statement

No potential conflict of interest was reported by the authors.

## Funding

This work was supported by the Sao Paulo Research Foundation (FAPESP) and the National Council for the Scientific and Technological Development (CNPq) for the financial support.

## ORCID

*A. F. Galvis* http://orcid.org/0000-0002-2833-2328

## References

Aliabadi, M. (2002). *The boundary element method: Applications in solids and structures* (Vol. 2). Chichester: John Wiley & Sons.

Bebendorf, M. (2000). Approximation of boundary element matrices. *Numerishce Mathematik, 86*, 565–589.

Bebendorf, M. & Rjasanow, S. (2003). Adaptive low-rank approximation of collocation matrices. *Computing, 70*, 1–24.

Benedetti, I., Milazzo, A., & Aliabadi, M. (2009). A fast dual boundary element method for 3D anisotropic crack problems. *International Journal for Numerical Methods in Engineering, 80*, 1356–1378.

Benedetti, I., Milazzo, A., & Aliabadi, M. (2011). Fast hierarchical boundary element method for large-scale 3-D elastic problems. In *Boundary element methods in engineering and sciences* (Vol. 4). Aliabadi, M. H., & Wen, P. H., Eds. London: Imperial College Press.

Borm, S., Grasedick, L., & Hackbusch, W. (2003). Introduction to hierarchical matrices with applications. *Engineering Analysis with Boundary Elements, 27*, 405–422.

Grasedyck, L. (2005). Adaptive recompression of H-matrices for BEM. *Computing, 74*, 205–223.

Grasedyck, L., & Hackbusch, W. (2003). Construction and arithmetics of H-matrices. *Computing, 70*, 295–334.

Kane, J. H. (1994). *Boundary element analysis in engineering continuum mechanics*. Englewood Cliffs, New Jersey: Prentice Hall.

Kurz, S., Rain, O., & Rjasanow, S. (2007). *Fast boundary element methods in computational electromagnetism*. Berlin: Springer.

Lee, V. (2003). Explicit expression of derivatives of elastic Green's functions for general anisotropic materials. *Mechanics Research Communications, 30*, 241–249.

Lee, V. G. (2009). Derivatives of the three-dimensional Green's function for anisotropic materials. *International Journal for Solids and Structures, 46*, 3471–3479.

Lifshitz, I. M., & Rozenzweig, L. N. (1947). Construction of the green tensor fot the fundamental equation of elasticity theory in the case of unbounded elastic anisotropic medium. *Zhurnal Éksperimental'noi i Teoreticheskoi Fiziki, 17*, 783–791.

Phan, P. V., Gray, L. J., & Kaplan, T. (2004). On the residue calculus evaluation of the 3-D anisotropic elastic green's function. *Communications In Numerical Methods In Engineering, 20*, 335–341.

Rodríguez, R., Galvis, A. F., Sollero, P., & Albuquerque, E. (2013). Analysis of multiple inclusion potential problems by the adaptive cross approximation method. *Computational Modeling in Engineering & Sciences, 96*, 259–274.

Rokhlin, H. (1985). Rapid solution of integral equation of classical potential theory. *Journal of Computational Physics, 60*, 187–207.

Sales, M. A., & Gray, L. J. (1998). Evaluation of the anisotropic green's function and its derivatives. *Computers & Structures, 69*, 247–254.

Shiah, Y. C., Tan, C. L., & Lee, V. G. (2008). Evaluation of explicit-form fundamental solutions for displacements and stresses in 3D anisotropic elastic solids. *Computer Modeling in Engineering & Science, 34*, 205–226.

Shiah, Y. C., Tan, C. L., & Lee, R. F. (2010). Internal point solutions for displacements and stresses in 3D anisotropic elastic solids using the boundary element method. *Computer Modeling in Engineering & Science, 69*, 167–197.

Shiah, Y. C., Tan, C. L., & Wang, C. Y. (2012). An efficient numerical scheme for the evaluation of the fundamental solution and its derivatives in 3D generally anisotropic elasticity. In *Advances in boundary element and meshless techniques XIII*, Prague. (pp. 190–199).

Soden, P. D., Hinton, M. J., & Kaddour, A. S. (1998). Lamina properties, lay-up configurations and loading conditions for a range of fibre-reinforced composite laminates. *Composite Science and Technology, 58*, 1011–1022.

Tan, C. L., Shiah, Y. C., & Lin, C. W. (2009). Stress analysis of 3D generally anisotropic elastic solids using the boundary element method. *Computer Modeling in Engineering & Science, 41*, 195–214.

Tan, C. L., Shiah, Y. C., & Wang, C. Y. (2013). Boundary element elastic stress analysis of 3D generally anisotropic solids using fundamental solutions based on fourier series. *International Journal of Solids and Structures, 50*, 2701–2711.

Tavara, L., Ortiz, J. E., Mantic, V., & Paris, R. (2008). Unique real-variable expression of displacement and traction fundamental solutions covering all transversely isotropic materials for 3D BEM. *International Journal for Numerical Methods in Engineering, 74*, 776–798.

Ting, T. C. T., & Lee, V. G. (1997). The three-dimensional elastostatic Green's function for general anisotropic linear elastic solids. *The Quarterly Journal of Mechanics & Applied Mathematics, 50*, 407–426.

Tonon, F., Pan, E., & Amadei, B. (2001). Green's functions and boundary element method formulation for 3D anisotropic media. *Computers & Structures, 79*, 469–482.

Wang, C. Y., & Denda, M. (2007). 3D bem for general anisotropic elasticity. *International Journal of Solids and Structures, 44*, 7073–7091.

Wilson, R., & Cruse, T. (1978). Efficient implementation of anisotropic three dimensional boundary-integral equation stress analysis. *International Journal for Numerical Methods in Engineering*, *12*, 1383–1397.